Supporting Information

Sarkar *et al.* 10.1073/pnas.0803103105

SI Text

Synthesis of Fluorescent Neurotensin and Construction of Neurotensin Receptor Library. A fluorescent neurotensin analog was prepared by coupling BODIPY FL-X, SE (Invitrogen) to the minimal bioactive peptide sequence NT(8–13) (AnaSpec) according to the manufacturer's instructions. The conjugated product was isolated by reverse-phase HPLC and purity was confirmed by mass spectrometry.

The initial NTR1 library was generated by epPCR using regular dNTPs (200 μM) and the nucleotide analogs dPTP and 8-oxo-dGTP (1–15 μM in different libraries, which were then combined, corresponding to 3–13 amino acid mutations, on average) (1). Library sequencing after the first four rounds of FACS revealed only 2 to 3 amino acid mutations per sequence; therefore, additional epPCR steps were only performed using 1 μM analogs. DNA shuffling in the last randomization step was performed using the StEP (2). The library complexity was $\approx 10^6$ to 10^7 initial transformants after each randomization step, and the library size screened during each round of FACS consisted of $\approx 10^7$ to 10^8 cells.

Optimization of Binding Buffer for Selections. Previous work by Georgiou and colleagues (3) suggested that the outer membrane of *E. coli* could be made permeable to relatively small ligands (<10 kDa) while retaining viability by using concentrated salt solutions. Because our NTR1 variants are functionally expressed in the inner membrane of *E. coli*, we tested the efficacy of several permeabilization buffers allowing binding of [^{3}H]-NT added to the extracellular medium (Fig. S1).

From a simple thermodynamic model that accounts for partitioning of ligand across a selective membrane, it can be shown from the above data that the ligand concentration in the periplasm is roughly one fifteenth that in the extracellular medium when 5× Tris-KCl is used (data not shown). Correspondingly, we predicted that expressed receptors would be essentially saturated in this buffer when 50 nM [^{3}H]-NT was used.

At this higher concentration of ligand, complete receptor saturation is achieved with the standard buffer and the extent of specific receptor binding is almost fully matched by the 5× Tris-KCl buffer (Fig. S2). Notably, Na^+ is a known inhibitor of NT in binding NTR1, so it is not surprising that the extent of receptor binding is reduced in the buffer containing high concentrations of Na^+. Additionally, divalent cations do not appear to maximize membrane permeability. Therefore, a buffer consisting of Tris and KCl was selected for further refinement. The influence of buffer concentration and composition on receptor binding (Fig. S3), enrichment ratios in FACS (Fig. S4), and viability of recovered cells after FACS (see Fig. S4) was determined. It is clear from Fig. S3 that Tris is critical for maximizing the signal, although more concentrated buffer solutions are not necessary. Then, cells incubated in the standard assay buffer, 5× Tris-KCl, 1× Tris, and 1× Tris-KCl were subject to FACS. To set the gating window, cells were incubated with saturating amounts of BODIPY-NT(8–13) but also with excess unlabeled NT(8–13), and the left boundary of the gating window was positioned just to the right of the cell populations for the standard buffer, 1× Tris, and 1× Tris-KCl (see Fig. S4). The 5× Tris-KCl buffer was not given further consideration, as it was evident from the scatter plots that the forward scatter (and thus the cell morphology) was significantly altered by the buffer. The signal-to-noise ratio in the gating window for the 1× Tris-KCl buffer was ≈900 and this buffer gave the best cell viability; therefore, it was chosen for all future experiments.

Flowchart for Selections. The procedure for performing selections for expression level and selectivity was as shown in Fig. S5.

Single-Clone Analysis After Selections. After the selections for expression and selectivity, individual clones were isolated for sequencing and expression. As outlined in Fig. S5, after the third round of epPCR and selection, enriched sequences were re-randomized either by a fourth round of epPCR or by shuffling through StEP and then screened for either maximal expression or ligand selectivity. Then, individual clones were chosen from each library in each of the selections [48 epPCR clones and 48 StEP clones in maximal expression (Fig. S6), and 48 of each in altered binding selectivity (Fig. S7)] and all 192 were compared to NTR1 for expression level by performing radioligand binding assays as outlined in *Methods*.

The properties of the best expressing clones from this analysis, D03 for maximal expression and G10 for altered ligand selectivity (both from 4EP03, not StEP), were also checked by flow cytometry (Figs. S8 and S9, respectively).

Amino Acid Mutations in D03 and G10. The positions of the evolved mutations in D03 are shown in the snake plot in Fig. S10. The location of the key selectivity mutation in G10 (F358S), which does not exist in D03, is also highlighted on this template.

Radioligand Binding Assays. Whole-cell binding assays with *E. coli* (20 μl culture) were performed with 380 μl of assay buffer [50 mM Tris·HCl, pH 7.4, 1 mM EDTA, 40 μg/ml bacitracin, 0.1% (wt/vol) BSA] containing a fixed concentration (10 nM) or dilution series (0.04–20 nM) of radioactive agonist [^{3}H]-NT (Perkin-Elmer), essentially as described (4). The expression culture was cooled to 4°C for at least 2 h before addition of assay buffer; thereafter, the mixed sample (culture plus assay buffer) was incubated at 4°C for an additional 2 h, centrifuged, washed and measured by scintillation counting. Nonspecific binding was determined in the presence of 5 μM unlabeled NT. Competition with antagonist SR 48692 (Sanofi Aventis) was determined at a concentration of 5 μM.

To measure binding to mammalian cells, cell pellets were resuspended in 500 μl of assay buffer with a fixed (2 nM) or increasing concentration of radioactive agonist [^{3}H]-NT (1–20 nM). Nonspecific binding was determined in the presence of 1 μM unlabeled NT. The cell suspension (250 μl) was incubated at room temperature for 20 min and the assay was terminated with 1 ml of ice-cold assay buffer and the free ligand was separated from bound ligand using 96-well filtration plates with glass-fiber filters (MAFBNOB, Millipore) pretreated with 0.5% (vol/vol) polyethylenimine and a vacuum filtration manifold (Millipore). OptiPhase HiSafe 2 scintillation mixture (Perkin-Elmer) was added directly to the wells (100 μl/well). The plate was shaken overnight and radioactivity was counted in a liquid scintillation counter (1450 Microbeta Plus, Perkin-Elmer).

Experiments with membranes from *P. pastoris* were performed similarly, but with a few modifications. The binding reaction took place in a thermomixer for 1 h at 30°C and 1,400 rpm in 250 μl binding buffer containing ≈70 μg of total membrane protein fractions (diluted with Tris-buffered saline (TBS) to ≈14 μg/μl) and 15 nM [^{3}H]-NT. Nonspecific binding was determined in the presence of 40 μM unlabeled NT. After

binding, 200 μl of membrane suspension was transferred to a 96-well filtration plate on the vacuum manifold. The filters were washed five times with 200 μl of cold assay buffer.

For solubilized receptor, an aliquot (1.5 μl) was incubated with 150 μl assay buffer containing 50 nM [^{3}H]-NT and detergents (0.05% (wt/vol) DDM, 0.5% (wt/vol) CHAPS, 0.1% (wt/vol) CHS; Anatrace) for 1.5 h at 4°C. Separation of receptor-ligand complex from free ligand was achieved with gel-filtration spin columns [Bio-Spin 30 (Tris buffer) column, Bio-Rad] preequilibrated with detergents. Radioactivity was measured by liquid scintillation counting.

***P. pastoris* Membrane Preparation.** For membrane preparations, cells were thawed on ice, and 5 ml of acid-washed glass beads (425–600 microns; Sigma-Aldrich) were added to the cell suspensions. Cell disruption was performed in three cycles (5 min at maximal speed, 5 min on ice to cool) in a TissueLyser (Qiagen). The membrane suspensions were transferred to 15-ml tubes and centrifuged at 4,000 × *g* for 15 min at 4°C to remove cell debris. The membrane suspensions were transferred to new tubes, and centrifuged at 150,000 × *g* for 30 min at 4°C. The membrane pellet was resuspended in 500 μl of ice-cold TBS containing 1% protease inhibitor mixture. The protein concentrations of the membrane preparations were determined by a Quant-iT Protein Assay Kit (Invitrogen) and the membrane suspensions were stored at −20°C.

Receptor Solubilization and Purification. Frozen cell pellets (−80°C) from 1 liter of expression culture (4–5 g) were thawed and resuspended in 10 ml 2× resuspension buffer (100 mM Tris·HCl, pH 7.4, 60% glycerol, 400 mM NaCl) with a disperser (IKA yellow line DI 18, 1 min, level 1). The following steps were carried out at 0–4°C. Protease inhibitors (mini complete protease inhibitors, EDTA-free, 1 tablet, Roche Applied Science), $MgCl_2$ (10 mM), DNase I (20 μg/ml, Roche Applied Science), and detergents [1.5% DDM; 0.5% CHAPS; 0.1% CHS] were added with gentle stirring. The volume was adjusted to 20 ml with ultrahigh purity water, sonicated for 3 min (Branson Sonifier 250, level 4, 30% duty cycle, ½-inch flat tip), and incubated for 2 h with gentle mixing. Cell debris was removed by centrifugation (20 min, 50,000 × *g*) followed by ultracentrifugation (45 min, 190,000 × *g*). Imidazole was then added to the clarified lysate to a final concentration of 50 mM, pH 7.8–7.9, before IMAC. Solubilized protein was passed at a flow rate of 0.3 ml/min over a 2-ml Superflow Ni^{2+}-NTA column (Qiagen) equilibrated with buffer NiA (50 mM Tris·HCl, pH 7.4, 30% glycerol, 200 mM NaCl, 50 mM imidazole, 0.1% DDM, 0.5% CHAPS, 0.1% CHS). The resin was washed with 15 column volumes of buffer NiA at a flow rate of 0.5 ml/min and the protein was eluted (0.2 ml/min) with buffer NiA containing 300 mM imidazole. For further purification by size exclusion chromatography (SEC), the collected peak fractions were pooled (4–5 ml) and concentrated to 250 μl (Amicon Ultra-4 50K, Millipore). The concentrated eluate was passed through a Superdex 200 column (GE Healthcare) equilibrated with buffer SEC15 (50 mM Tris·HCl, pH 7.4, 15% glycerol, 1 M NaCl, 1 mM EDTA, 0.05% DDM, 0.5% CHAPS, 0.1% CHS) at a flow rate of 0.3 ml/min. All chromatography steps were performed on an Äkta Prime system (GE Healthcare). Radioligand binding assays with solubilized receptor were performed as described above.

All variants tested bind quantitatively to a NT-affinity column (data not shown) (4), but D03 evolved to be refractive to competition with Na^+ and could therefore not be eluted from this column with high salt. That binding to the affinity column (monomeric avidin saturated with biotinylated NT) is indeed because of productive binding of ligand was shown by specifically eluting bound receptor with an excess of free biotin (data not shown). Consequently, affinity purification was omitted for comparative purposes, as elution with Na^+ was not possible for all variants.

$[Ca^{2+}]_i$ Signaling Patterns Mediated by NT. Common features of NT signaling that have been recognized are activation of phospholipase C (PLC), production of inositol-1,4,5-trisphosphate, and mobilization of intracellular calcium ($[Ca^{2+}]_i$), suggesting that this receptor is coupled to $G_{q/11}$ protein (5, 6). Activation of PLC-coupled GPCRs can trigger a variety of Ca^{2+} signaling patterns (7), and the nature of the resulting signal depends on factors such as cell type, extracellular concentration of Ca^{2+}, and choice of agonist and its concentration. At the lowest agonist concentrations at which any signaling is observed in HEK293T cells expressing NTR1 or its mutants, application of NT predominantly induced sinusoidal $[Ca^{2+}]_i$ oscillations. Oscillations in $[Ca^{2+}]_i$ have been observed during signal transduction for a wide variety of receptors (8, 9); these fluctuations may enable frequency-dependent cellular responses as opposed to amplitude-dependent responses, which would require sustained exposure to elevated $[Ca^{2+}]_i$. At higher concentrations, a strong but transient response (no oscillations) is observed. At supersaturating concentrations of agonist, maximal release of Ca^{2+} is achieved. This is then followed by store-depletion gated Ca^{2+} influx, resulting in typical plateau-shaped $[Ca^{2+}]_i$ response curves (10).

The increase in $[Ca^{2+}]_i$ upon agonist binding was measured in single-cell experiments, as described in *Methods*. Upon stimulation, three different types of response were observed at the single-cell level, even at a given concentration of agonist (Fig. S11).

The three responses are characterized as plateau, transient, and oscillatory. A plateau response (bold green trace in Fig. S11) is defined as one in which the fluorescence ratio does not decrease to the baseline value but remains at a value at least 30% of the peak maximum 90 seconds after treatment with agonist has been stopped. It has been suggested that this type of response is caused mainly by the influx of Ca^{2+} from the extracellular space (11). The plateau response occurs primarily at very high NT concentrations. At intermediate agonist concentrations, only minimal depletion of Ca^{2+} stores is thought to occur, and therefore a plateau response is less common. A transient response (bold blue trace in Fig. S11) is defined as one in which the fluorescence ratio increases shortly after receptor activation and returns approximately to the baseline value within 60 s. Finally, an oscillatory response is defined as one in which multiple transient responses arise within a period of 180 to 200 s after agonist activation. Oscillations in $[Ca^{2+}]_i$ occur under a variety of conditions and play functional roles in signal transduction and cell regulation (12). They typically arise from calcium-induced calcium release mechanisms, in which an increase in $[Ca^{2+}]_i$ leads to increased Ca^{2+} influx from intracellular Ca^{2+} stores (13). In this experimental system, the observed oscillations differed in both frequency and intensity. Most oscillating responses occurred at low (0.1 nM or less) neurotensin concentrations and disappeared almost entirely at high agonist concentrations (10 nM or more).

While plateau, transient, and oscillatory responses all exist at a given concentration of agonist, the likelihood of observing a particular type of response changes with the type of receptor and the agonist concentration (see main text and Fig. 3).

The selection of NTR1 variants was performed on N-terminally truncated receptor (amino acids 43–424). Therefore, receptor expression and signaling in mammalian cells were also performed with truncated versions. However, to show that receptor truncation does not alter the intrinsic signaling patterns, full-length NTR1 (NTR1fl) and D03 (D03fl) were constructed using a synthetic gene for the N-terminal domain. No major difference between the truncated and full-length forms was

detected. Oscillations are most dominant at low agonist concentrations (0.01 nM), and larger fractions of transient and plateau responses are observed as the agonist concentration is increased (see Fig. 3 and Fig. S12).

Expression of NTR1 Variants in *E. coli* and *P. pastoris*. To compare total GPCR biosynthesis per bacterial cell, NTR1, D03, and D03-L167R were expressed in parallel *E. coli* cultures, which were then lysed and probed for total full-length receptor fusion by whole-cell Western blotting (Fig. S13). The order-of-magnitude increases in D03 and D03-L167R expression levels seen in this blot (a measure of all full-length receptor molecules per cell) are in good agreement with the respective 8.7- and 6.6-fold increases observed by radioligand binding assay (a measure of folded, functional receptor in the inner bacterial membrane; see Table 1 in main text).

The enhanced expression of D03 that is observed in *P. pastoris* could result either from an intrinsic increase in protein biosynthesis of this variant or from more efficient folding after translocation and processing. To address this, we detected the precursor form of NTR1, D03, and D03-L167R expressed in *P. pastoris* by Western blot (Fig. S14).

Because this precursor form is detected at a similar intensity for all samples (except the "ctrl"), it is reasonable to conclude that the order-of-magnitude increase in expression for D03 in *P. pastoris* arises primarily from more efficient folding and not from enhanced biosynthesis.

Influence of Point Mutation in Expression Vector Backbone. During selection, a mutation close to the origin of replication in the expression vector (Fig. S15). To determine what effect, if any, this mutation [C7054G; position 1 corresponding to the first G nucleotide of the *lacI*^{q} gene of the vector pRG/III-hs-MBP (14)] might have on plasmid copy number and receptor expression, NTR1 and D03 were cloned into the original vector (denoted pRG_{WT}) and the mutant vector (denoted pRG_{C7054G}) (Fig. S16).

Based on Fig. S16, it is clear that the C7054G point mutation increases plasmid copy number. However, this increase in DNA content does not correlate to any increase in functional NTR1 protein expression, suggesting that other, more significant bottlenecks exist along the biosynthetic pathway. Conversely, the corresponding increase in D03 DNA does result in only ≈25% more functional protein, implying that other bottlenecks along the biosynthetic pathway have been at least partially alleviated by the improved biophysical properties of the D03 sequence.

Gel Filtration of NTR1 and D03. Gel filtration was performed on detergent-solubilized, purified NTR1 and D03 to compare the two elution profiles. As shown in Fig. S17, the two traces are virtually identical with respect to the dominant peak (V_e = 11.9 ml).

To further confirm that the dominant protein peak does indeed contain functional receptor, radioligand-binding assays were performed (as described above) with sample fractions that were collected from this peak. The result for D03 is given in Fig. S8, which directly shows that the amount of functional receptor in each collected fraction closely mirrors the absorbance signal of the eluate at the corresponding elution volume.

Effect of Additive and Subtractive Point Mutations in NTR1 and D03, Respectively. To ascertain how isolated amino acid substitutions might affect the expression of NTR and D03, each mutation in D03 was singly introduced into NTR1 and, similarly, each mutation in D03 was reverted back to the WT residue. Using whole-cell binding assays with saturating amounts of radioligand (see above), the expression level of these 28 NTR1 variants in *E. coli* was determined (Fig. S19). As seen in this figure, the effect of each substitution on expression level is relatively small. Nevertheless, the sum of these multiple minor enhancements results in a variant, D03, with an order-of-magnitude increase in expression level; we refer to this phenomenon as a "staircase effect." This is in stark contrast to single amino acid substitutions that have a dramatic impact on phenotype, as in the case of the selectivity variant G10 (see main text); we refer to this phenomenon as an "elevator effect."

1. Zaccolo M, Gherardi E (1999) The effect of high-frequency random mutagenesis on in vitro protein evolution: A study on TEM-1 β-lactamase. *J Mol Biol* 285:775–783.
2. Zhao H, Giver L, Shao Z, Affholter JA, Arnold FH (1998) Molecular evolution by staggered extension process (StEP) in vitro recombination. *Nat Biotechnol* 16:258–261.
3. Chen G, *et al.* (2001) Isolation of high-affinity ligand-binding proteins by periplasmic expression with cytometric screening (PECS). *Nat Biotechnol* 19:537–542.
4. Tucker J, Grisshammer R (1996) Purification of a rat neurotensin receptor expressed in. *Escherichia coli Biochem J* 317:891–899.
5. Kitabgi P (2006) Functional domains of the subtype 1 neurotensin receptor (NTS1). *Peptides* 27:2461–2468.
6. Hermans E (2003) Biochemical and pharmacological control of the multiplicity of coupling at G-protein-coupled receptors. *Pharmacol Ther* 99:25–44.
7. Rovati GE, Capra V, Neubig RR (2007) The highly conserved DRY motif of class A G protein-coupled receptors: Beyond the ground state. *Mol Pharmacol* 71:959–964.
8. Hu Q, Deshpande S, Irani K, Ziegelstein RC (1999) $[Ca^{2+}]_i$ oscillation frequency regulates agonist-stimulated NF-κB transcriptional activity. *J Biol Chem* 274:33995–33998.
9. Berridge MJ, Lipp P, Bootman MD (2000) The versatility and universality of calcium signaling. *Nat Rev Mol Cell Biol* 1:11–21.
10. Liu X, Ambudkar IS (2001) Characteristics of a store-operated calcium-permeable channel: Sarcoendoplasmic reticulum calcium pump function controls channel gating. *J Biol Chem* 276:29891–29898.
11. Suh SH, *et al* (1999) Characterisation of explanted endothelial cells from mouse aorta: Electrophysiology and Ca^{2+} signalling. *Pflügers Arch* 438:612–620.
12. Berridge MJ, Bootman MD, Roderick HL (2003) Calcium signalling: Dynamics, homeostasis and remodeling. *Nat Rev Mol Cell Biol* 4:517–529.
13. Goldbeter A, Dupont G (1990) Allosteric regulation, cooperativity, and biochemical oscillations. *Biophys Chem* 37:341–353.
14. White JF, Trinh LB, Shiloach J, Grisshammer R (2004) Automated large-scale purification of a G protein-coupled receptor for neurotensin. *FEBS Lett* 564:289–293.

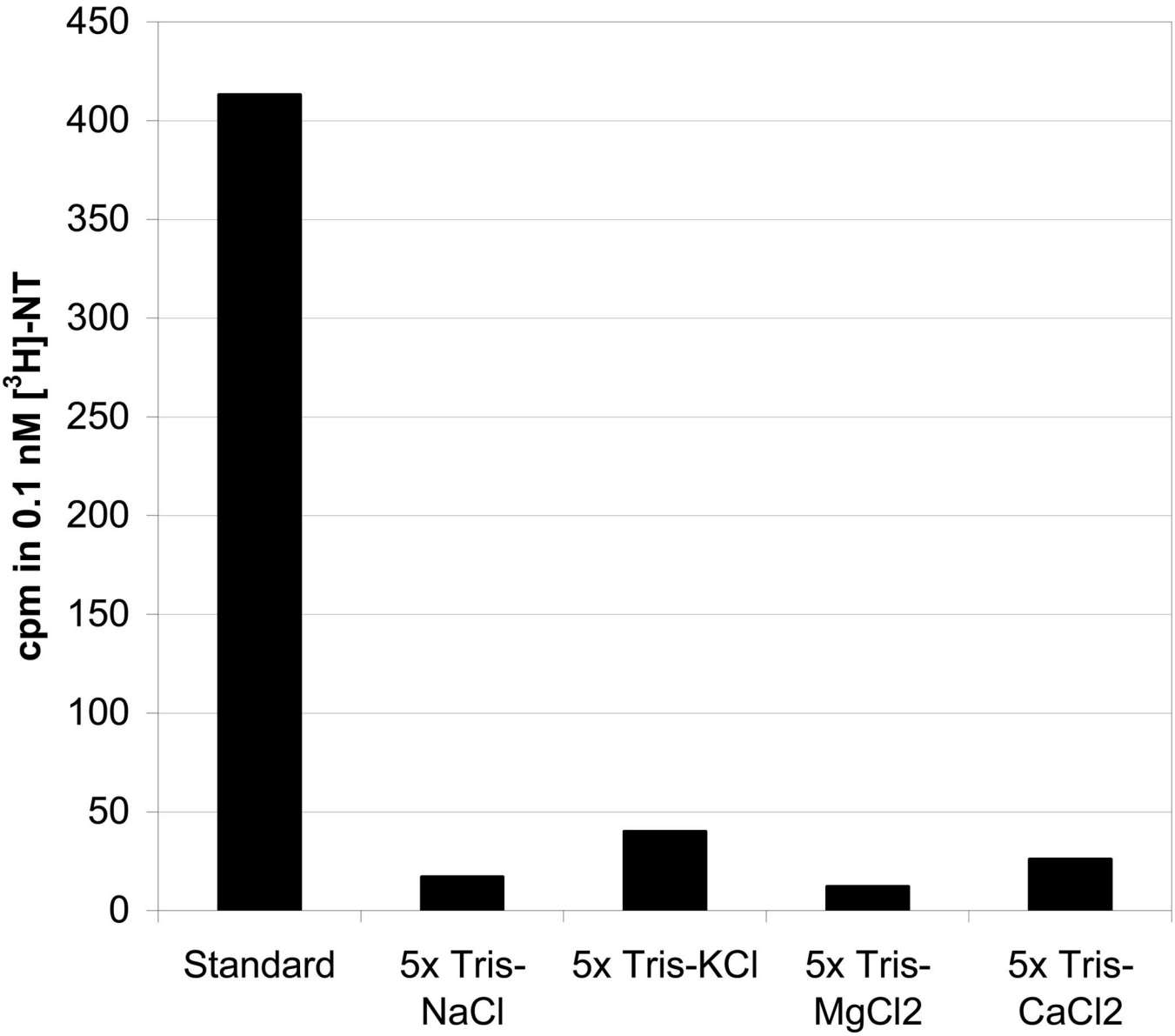

Fig. S1. Specific binding of 0.1 nM [^{3}H]-NT to cells expressing NTR1 in the specific buffers. ''Standard'' is the normal binding assay buffer, defined in the *Methods* section, and contains 1 mM EDTA, which renders the outer membrane fully permeable. A 5× buffer formulation comprises 250 mM Tris, 750 mM chloride salt, pH 7.4. Note that the extracellular ligand concentration used here is approximately the K_D value.

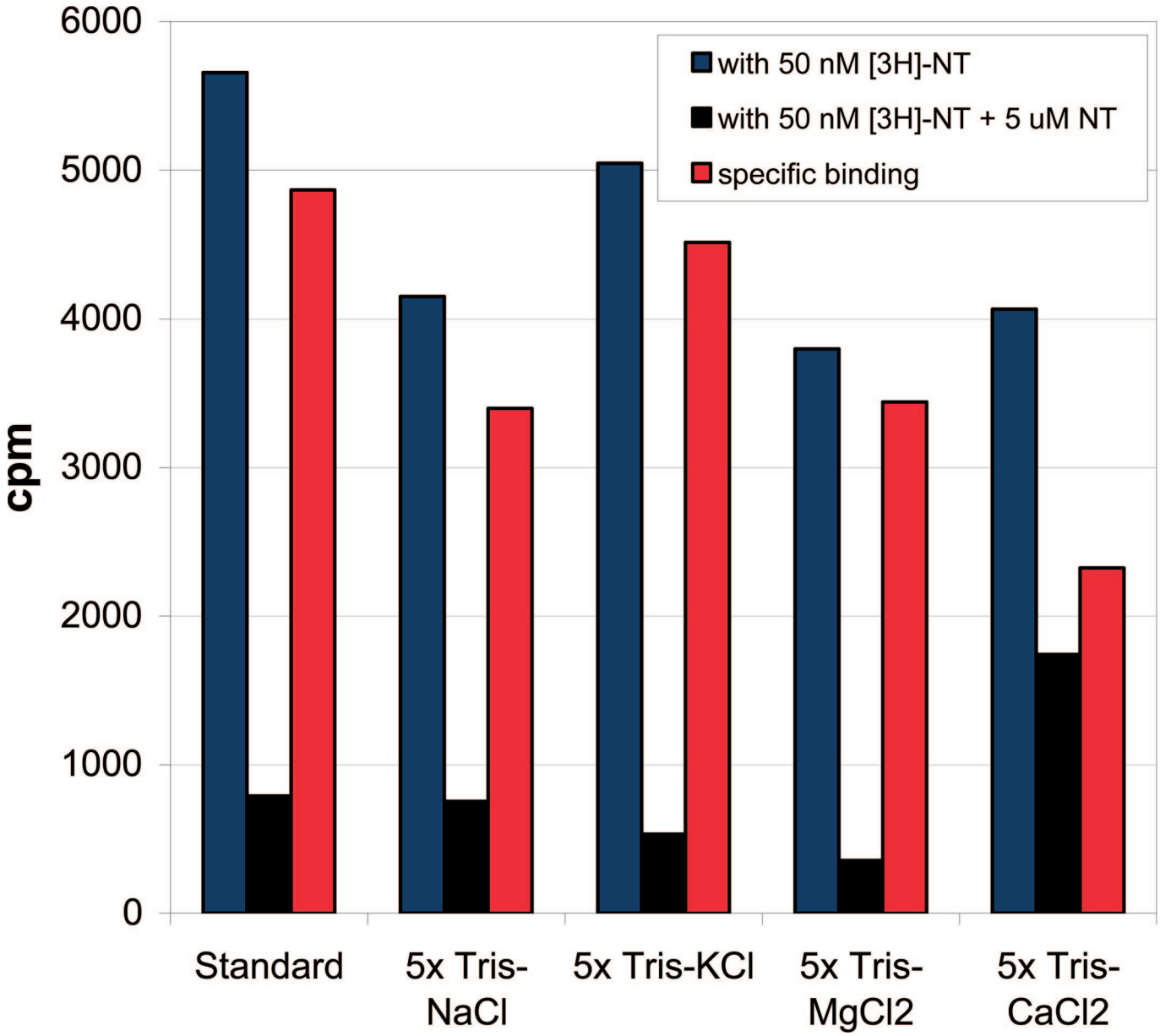

Fig. S2. Total, nonspecific, and specific binding of 50 nM [^{3}H]-NT to cells expressing NTR1 in the specific buffers. ''Standard'' is the normal binding assay buffer, defined in the *Methods* section, and contains 1 mM EDTA, which renders the outer membrane fully permeable. A 5× buffer formulation comprises 250 mM Tris, 750 mM chloride salt, pH 7.4.

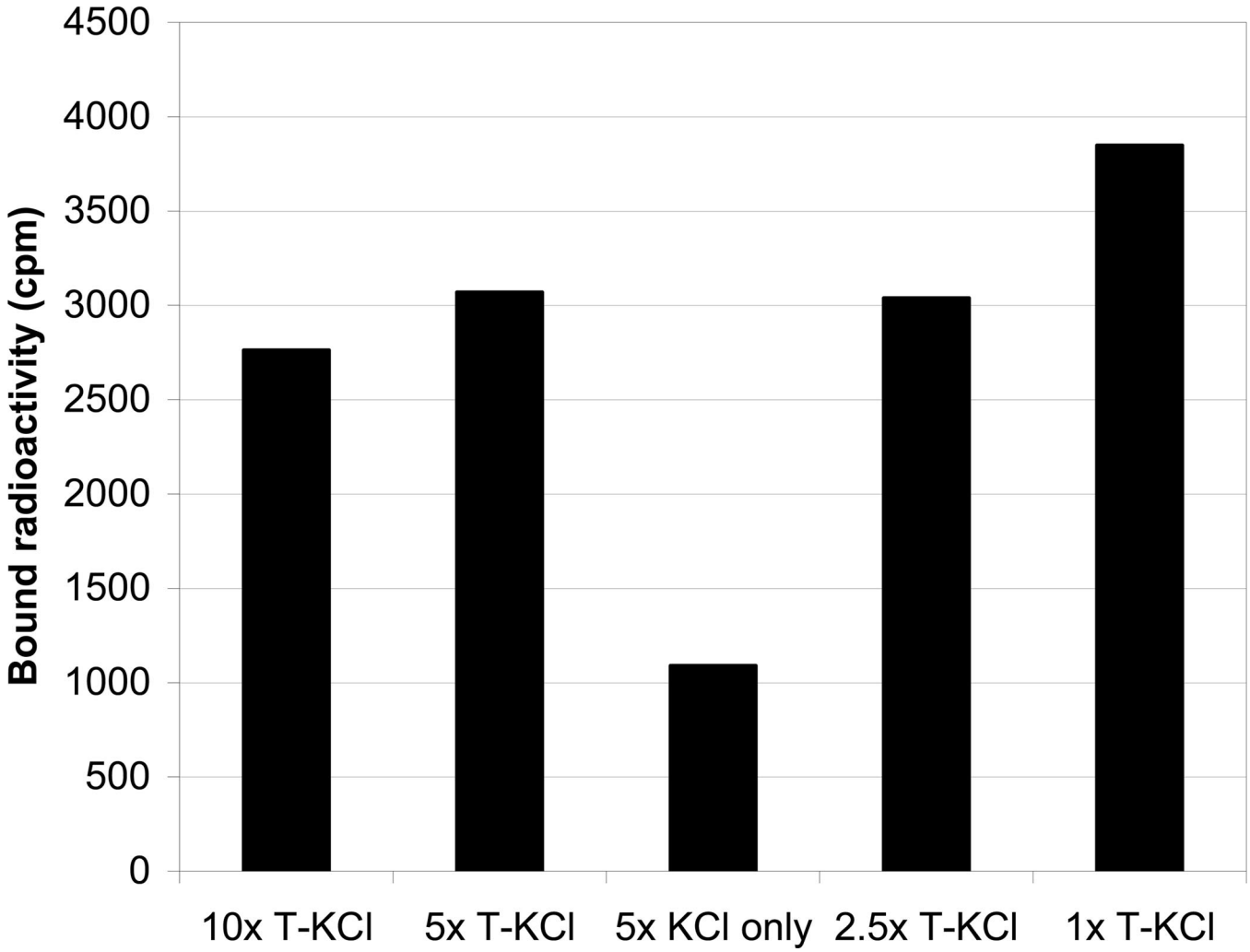

Fig. S3. Influence of buffer concentration (and composition) on specific binding of 50 nM [^{3}H]-NT to cells expressing NTR1. Note that Tris (abbreviated ''T'') is critical for efficient permeabilization of the outer membrane, as evidenced by the sample with 5× KCl only.

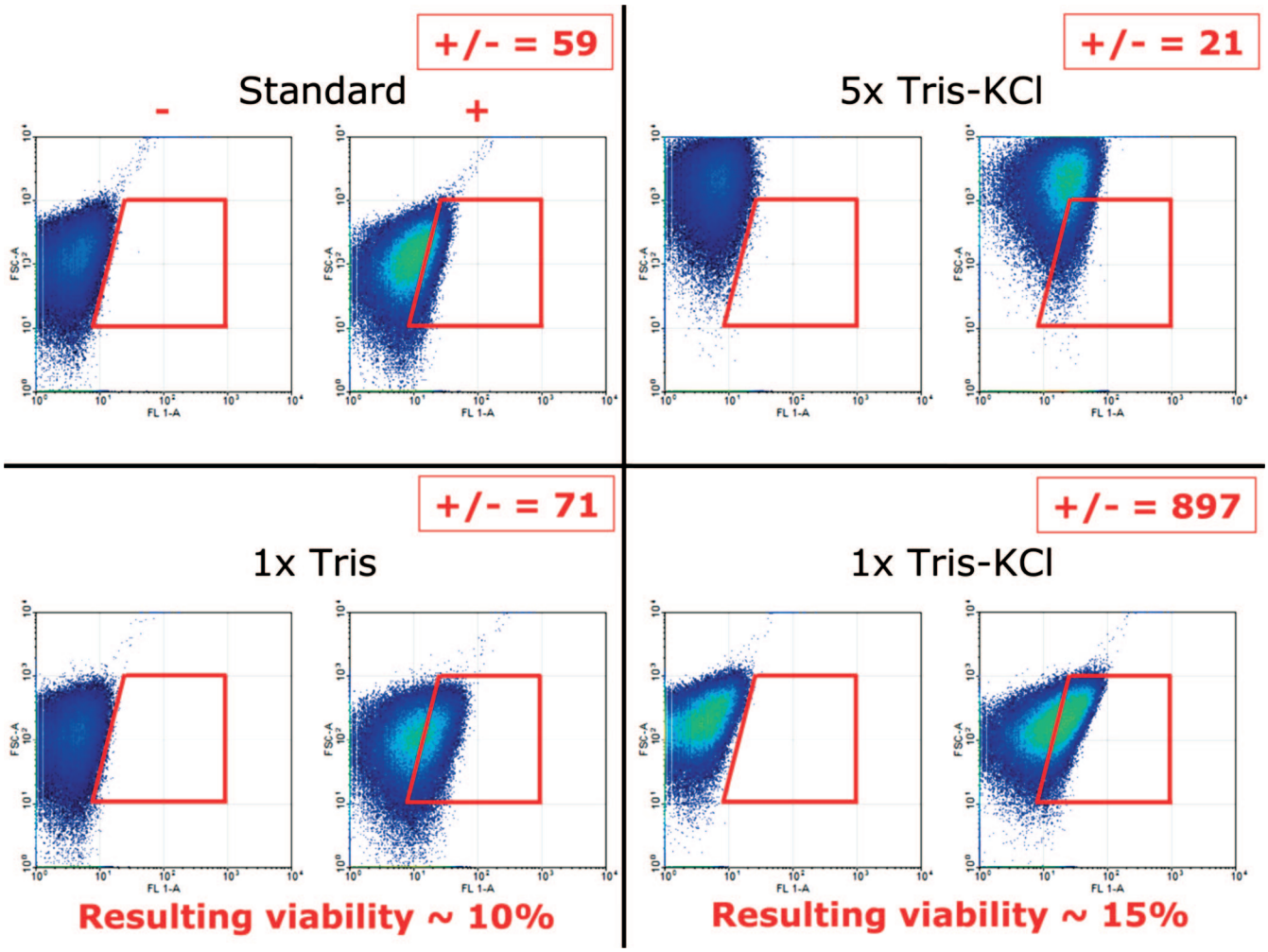

Fig. S4. Influence of buffer concentration and composition on enrichment ratios in a specified gate in FACS. Scatter plots show green fluorescence on the *x*-axis and forward scatter on the *y*-axis. The same gate was used in all eight samples shown. In comparison to the other samples, the 5× Tris-KCl buffer appeared to alter cell morphology, as detected by shifted forward scatter. Cell viability was determined by dispensing an aliquot of recovered cells from FACS onto ampicillin-containing agar plates and comparing the number of viable colonies to the expected number of cells in that volume.

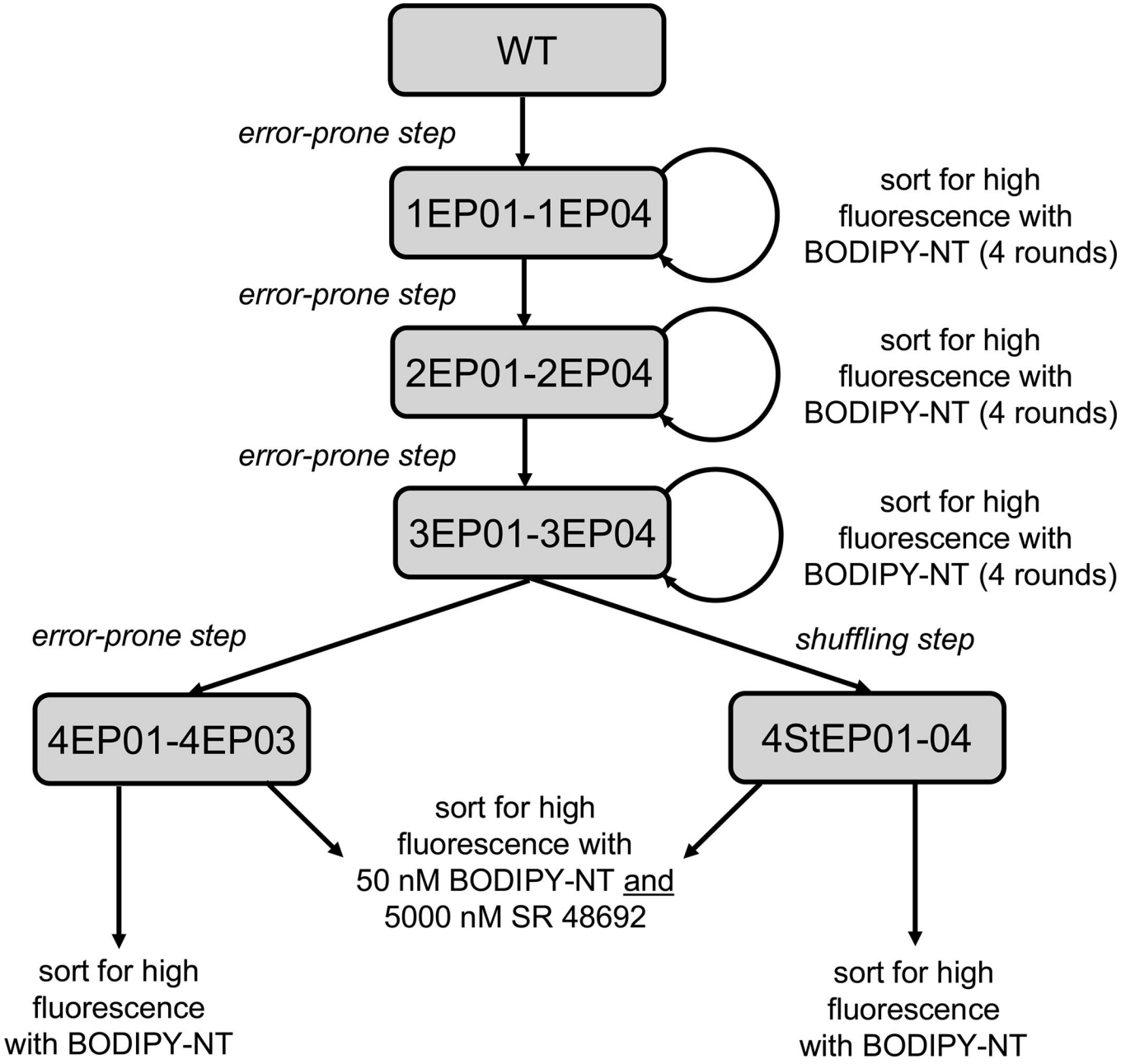

Fig. S5. Flowchart for selections of NTR1 variants with increased expression level or altered ligand selectivity.

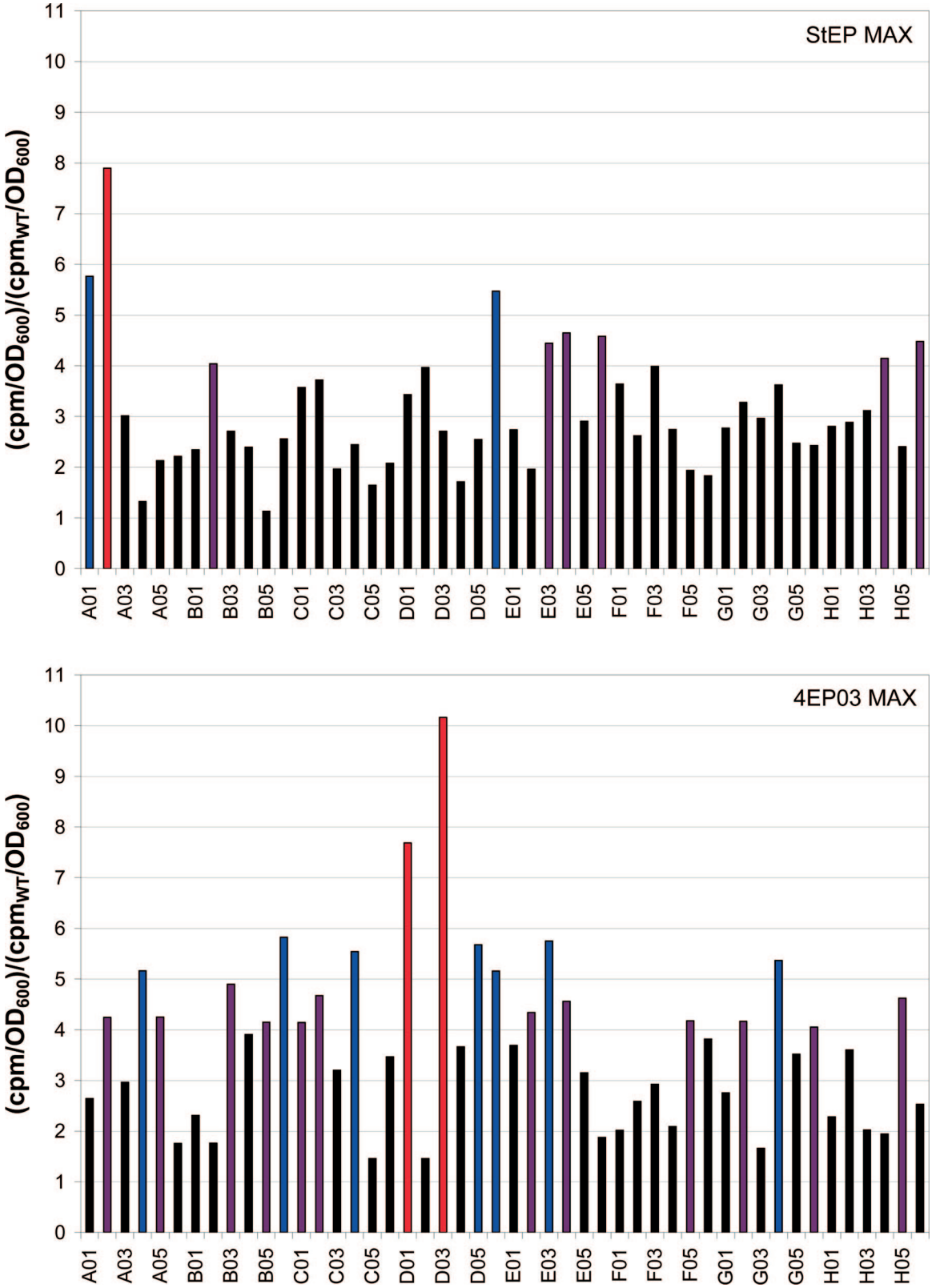

Fig. S6. Radioligand binding analysis of 96 clones isolated from selections for maximum receptor expression level. The *y*-axis represents receptor expression level relative to wild-type NTR1 expression level. The 48 clones in the top plot were chosen from the StEP library; the 48 in the bottom from the epPCR library. Purple bars represent clones with expression levels at least fourfold that of NTR1; blue bars at least fivefold; and red bars at least sevenfold. D03 from 4EP03 MAX is the clone with the highest expression level in this experiment (10-fold that of NTR1).

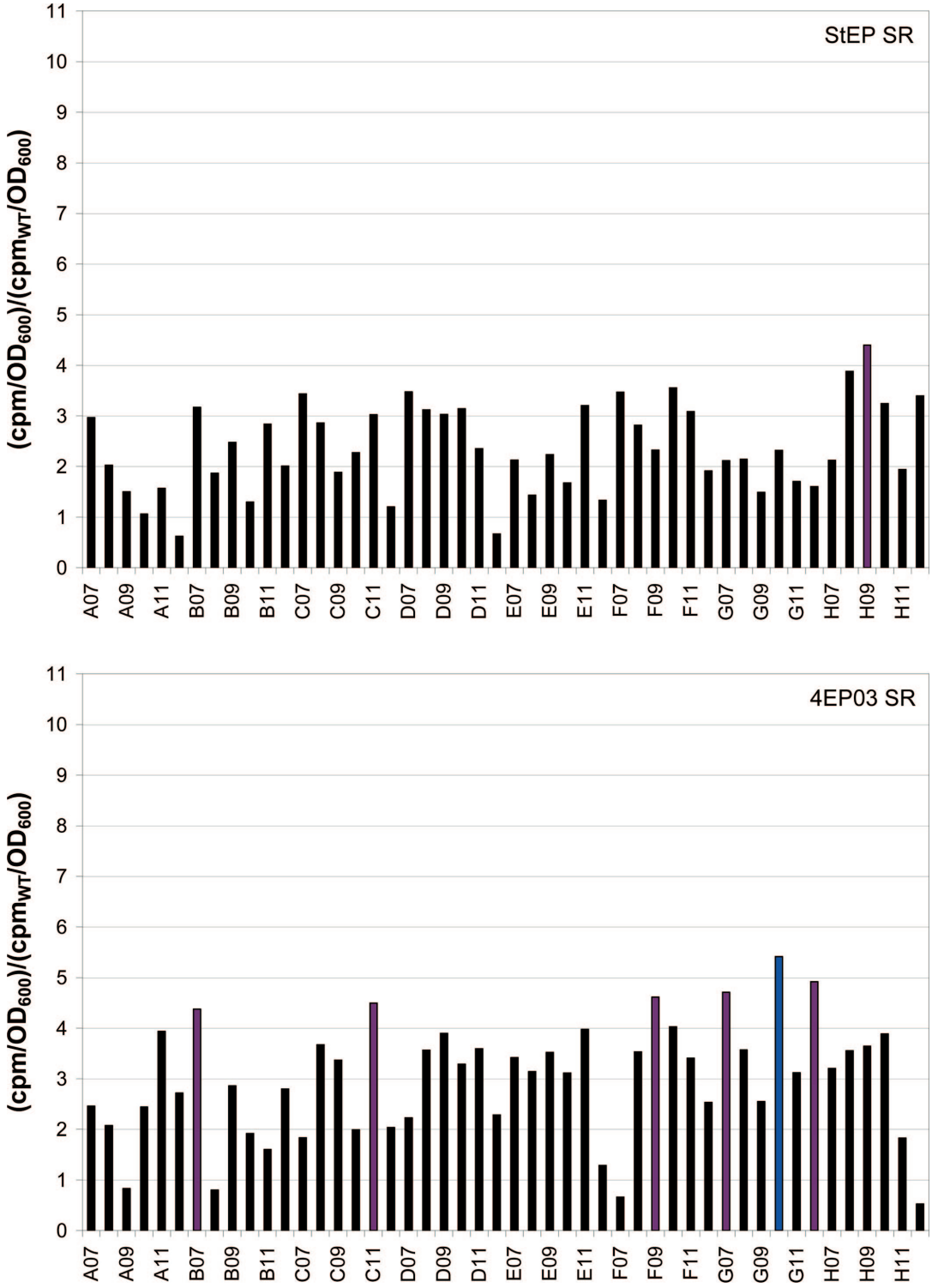

Fig. S7. Radioligand binding analysis of 96 clones isolated from selections for altered ligand selectivity. The *y*-axis represents receptor expression level relative to WT NTR1 expression level. The 48 clones in the top plot were chosen from the StEP library; the 48 in the bottom from the epPCR library. Purple bars represent clones with expression levels at least fourfold that of NTR1 and blue bars at least fivefold. G10 from 4EP03 SR is the clone with the highest expression level in this experiment (fivefold that of NTR1).

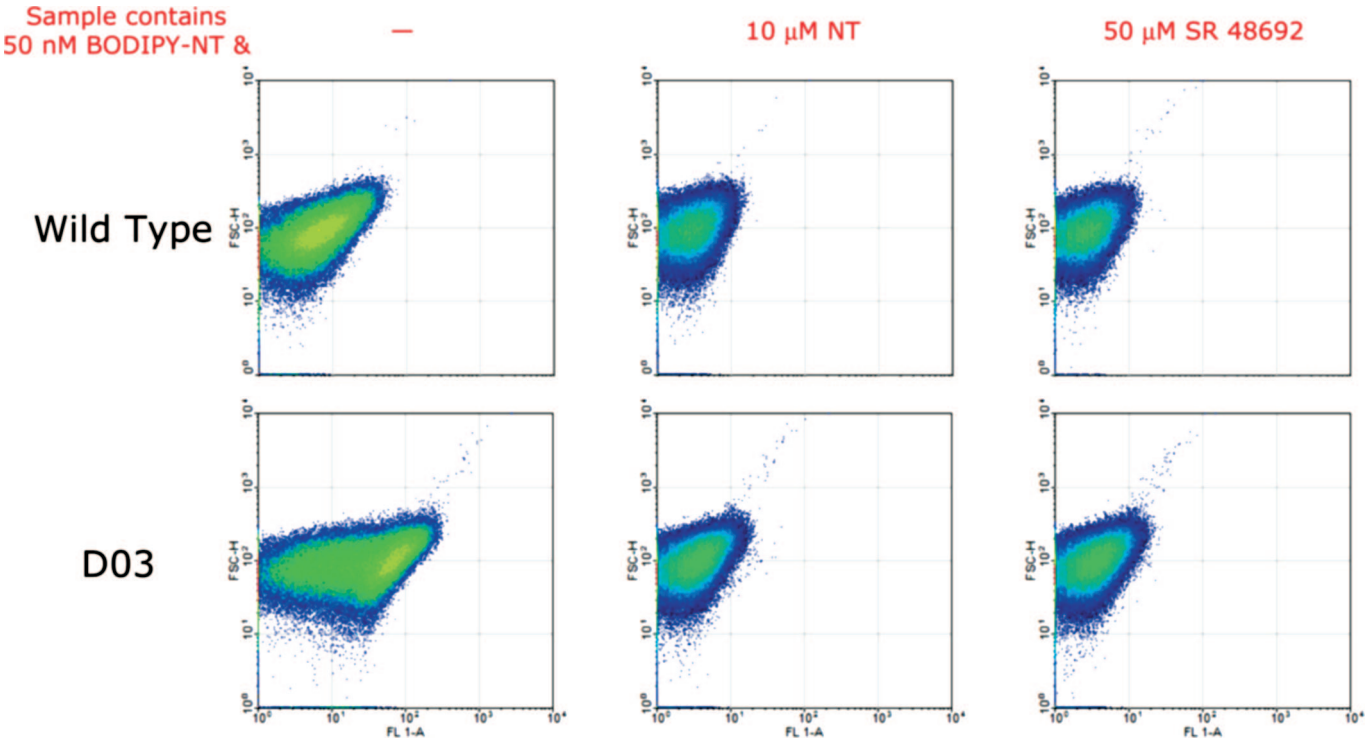

Fig. S8. Flow cytometric analysis of D03 compared to WT NTR1. The mean fluorescence signal obtained for D03 in the presence of saturating BODIPY-NT alone is an order of magnitude greater than that of NTR1. However, this signal can be fully competed by addition of either excess NT or excess SR 48692.

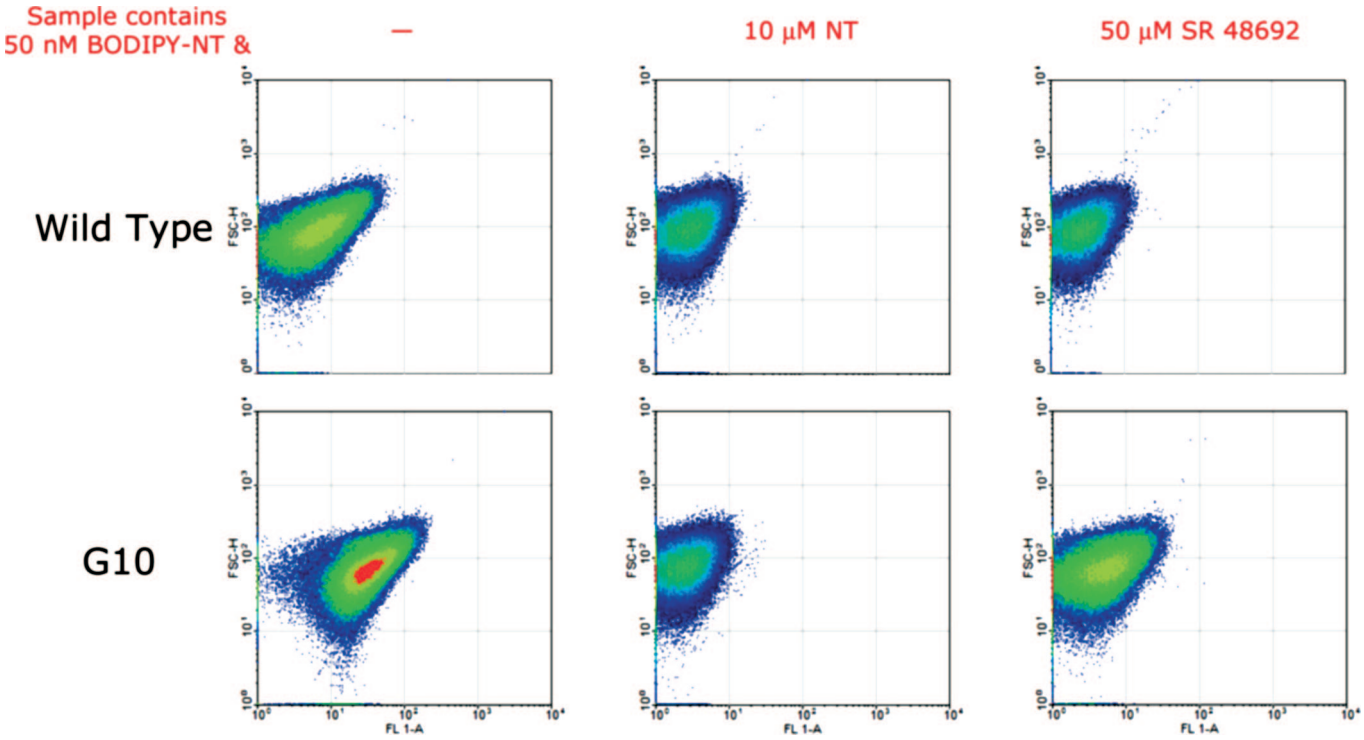

Fig. S9. Flow cytometric analysis of G10 compared to WT NTR1. The mean fluorescence signal obtained for G10 in the presence of saturating BODIPY-NT alone is approximately fivefold that of NTR1. This fluorescence signal can be fully competed by addition of excess NT; however, addition of excess SR 48692 does not achieve full inhibition.

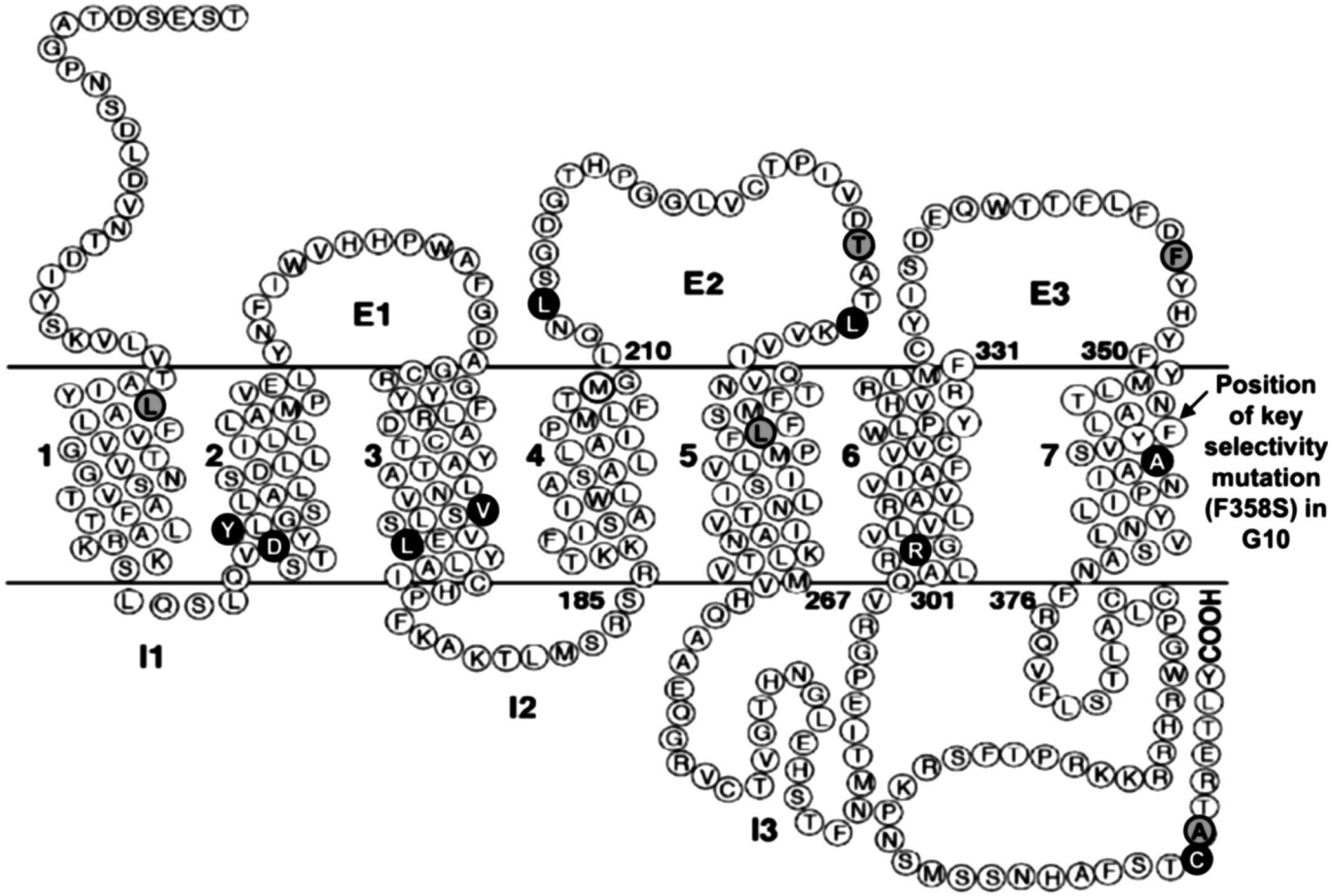

Silent mutations

Leu72 (CTG) → Leu (CTA^{rare})
Thr231 (ACA) → Thr (ACT)
Leu247 (CTG) → Leu (CTA^{rare})
Phe346 (TTC) → Phe (TTT)
Ala418 (GCC) → Ala (GCT)

Non-silent mutations

His103 (CAT) → Asp (GAT)
His105 (CAC) → Tyr (TAC)
Ala161 (GCC) → Val (GTC)
Arg167 (CGC) → Leu (CTC)
Arg213 (CGC) → Leu (CTC)
Val234 (GTC) → Leu (CTC)
His305 (CAC) → Arg (CGC)
Ser362 (TCC) → Ala (GCC)
Ser417 (AGC) → Cys (TGC)

Fig. S10. Snake plot of NTR1 (5) highlighting the silent (gray) and nonsilent (black) mutations in D03. The location of the key selectivity mutation in G10 (F358S) is also highlighted on this plot, although this mutation does not exist in D03.

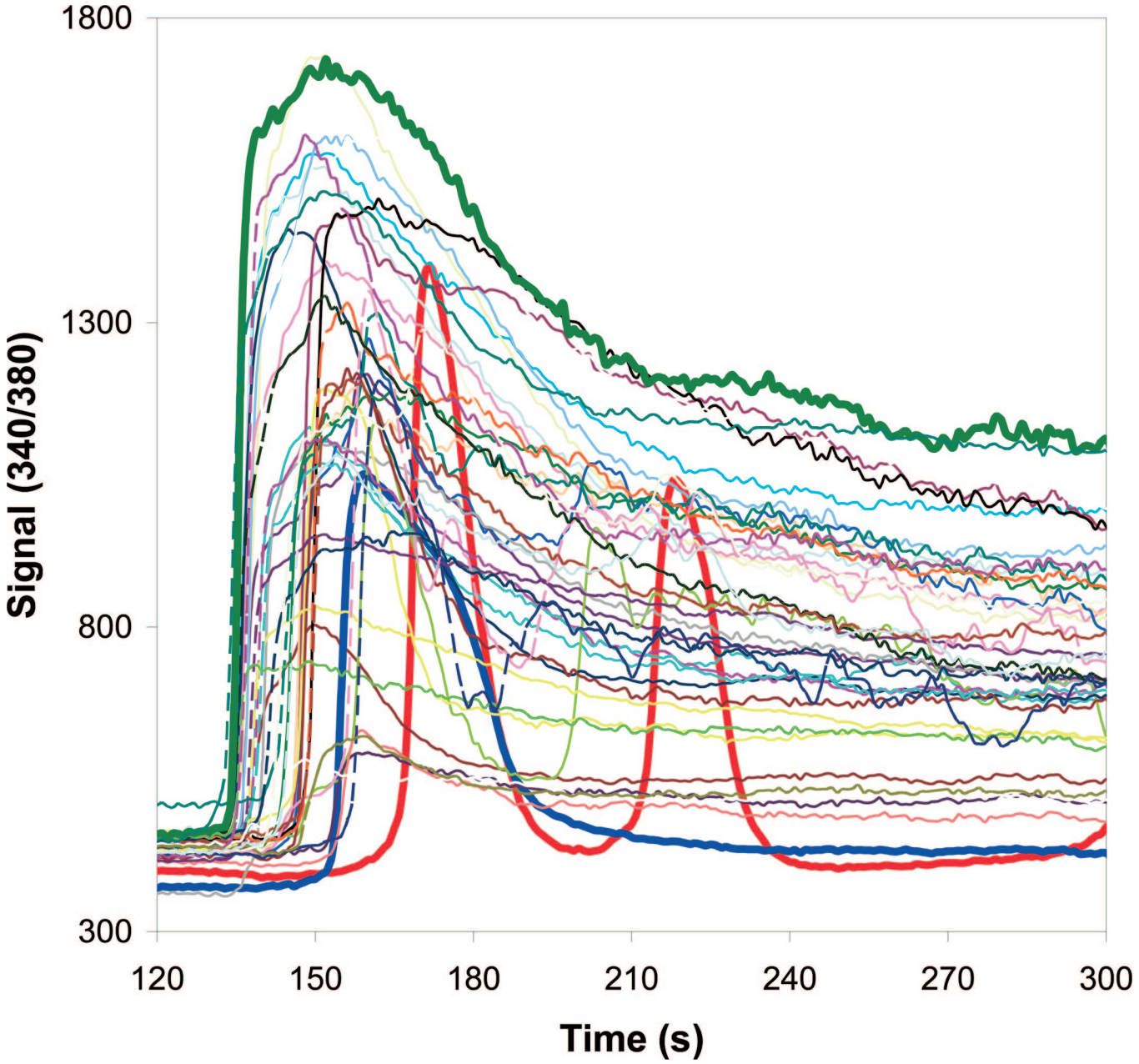

Fig. S11. Variation in cytosolic calcium levels in individual HEK293T cells in response to 1 nM NT. Each trace represents a single cell and is characterized as plateau (bold green), transient (bold blue), or oscillatory (bold red).

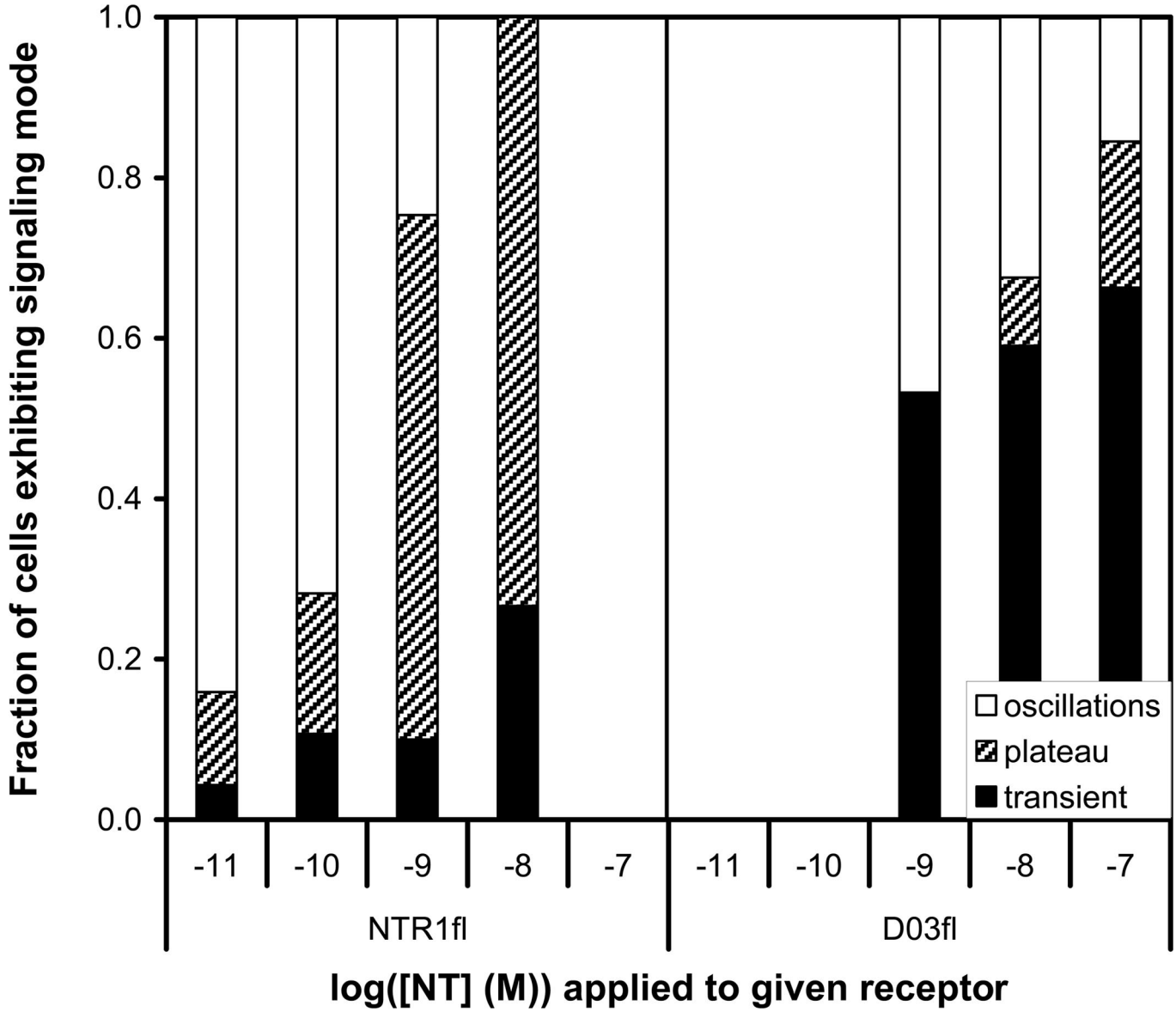

Fig. S12. Ca^{2+} signaling in HEK293T cells expressing NTR1fl or D03fl (fl, full length, i.e., no N-terminal truncation). A comparison with Fig. 3 in the main text suggests that the N-terminal truncation has minimal effect on the nature of signal transduction through these receptors. Oscillatory, plateau, and transient responses are illustrated in Fig. S11 and defined in the *SI Text*.

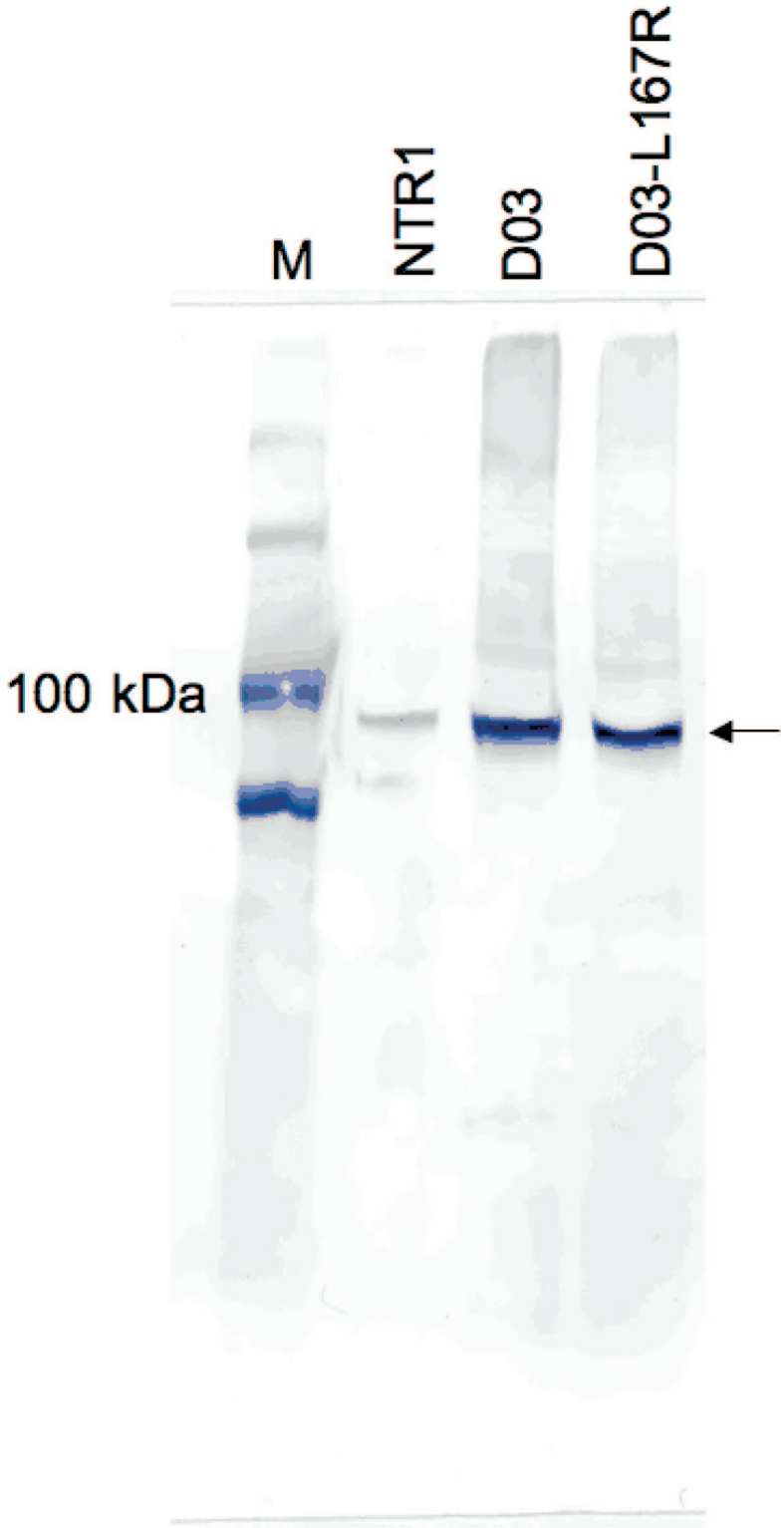

Fig. S13. Whole-cell Western blot of NTR1, D03, and D03-L167R expressed in *E. coli*. Each lane was loaded with 5 μl of cell suspension (adjusted to OD_{600} = 25). The C-terminal His_{10} tag was detected with a primary mouse anti-His_4 antibody and a secondary anti-mouse IgG alkaline phosphatase conjugate. The arrow indicates the recombinant fusion protein (MBP-GPCR-TrxA-His_{10}) with the expected molecular mass of 100.2 kDa.

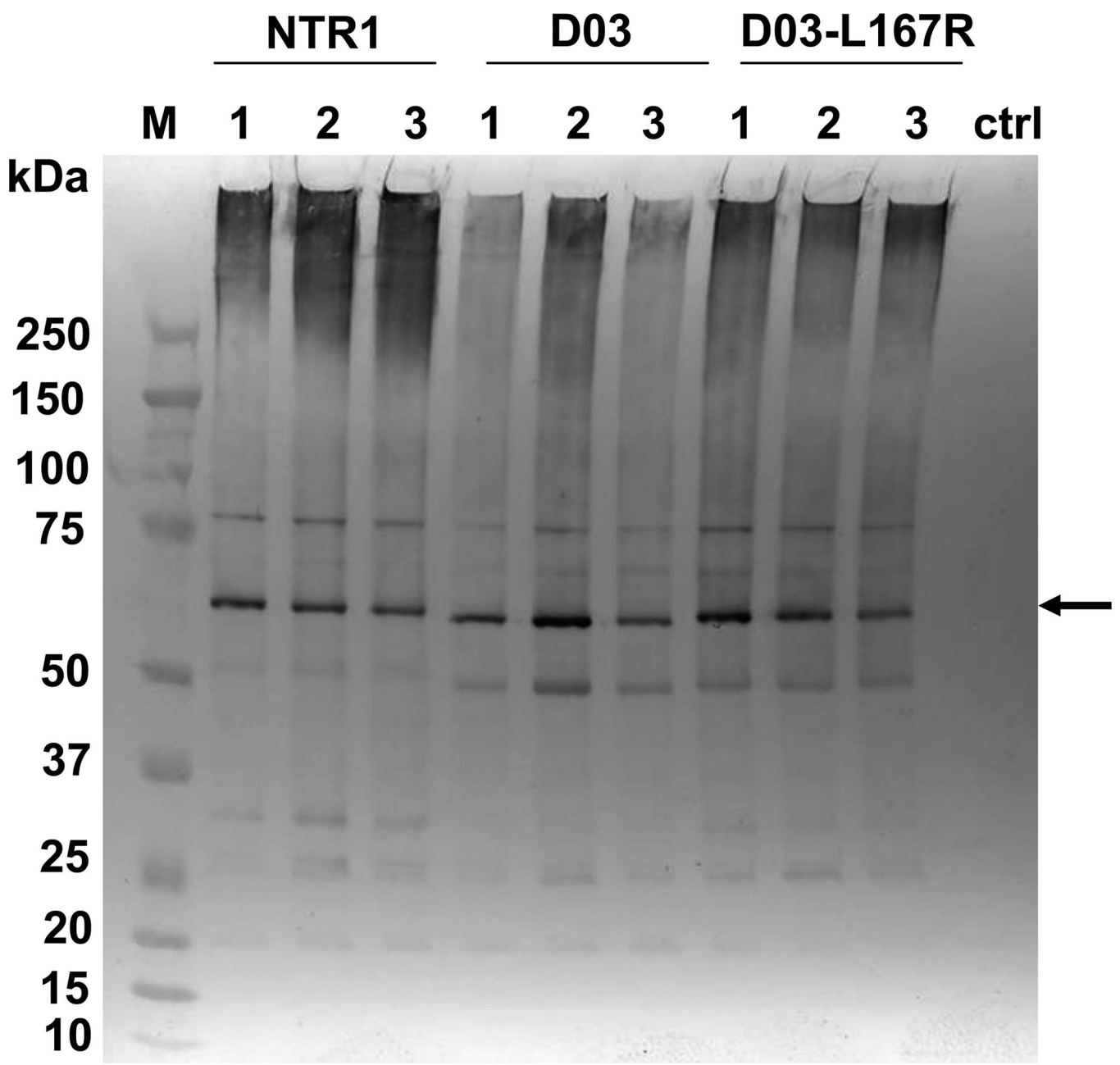

Fig. S14. NTR1, D03, and D03-L167R were analyzed by Western blot. In each lane, ≈20 μg of total membrane protein was loaded. The GPCR precursor form was detected with anti-prepro-α-factor antiserum [primary; courtesy of Randy Schekman (University of California, Berkeley)] and alkaline phosphatase conjugated goat anti-rabbit-IgG (secondary). The arrow on the right of the blot denotes the size corresponding to this precursor form. The negative control (ctrl) lacks a GPCR insert.

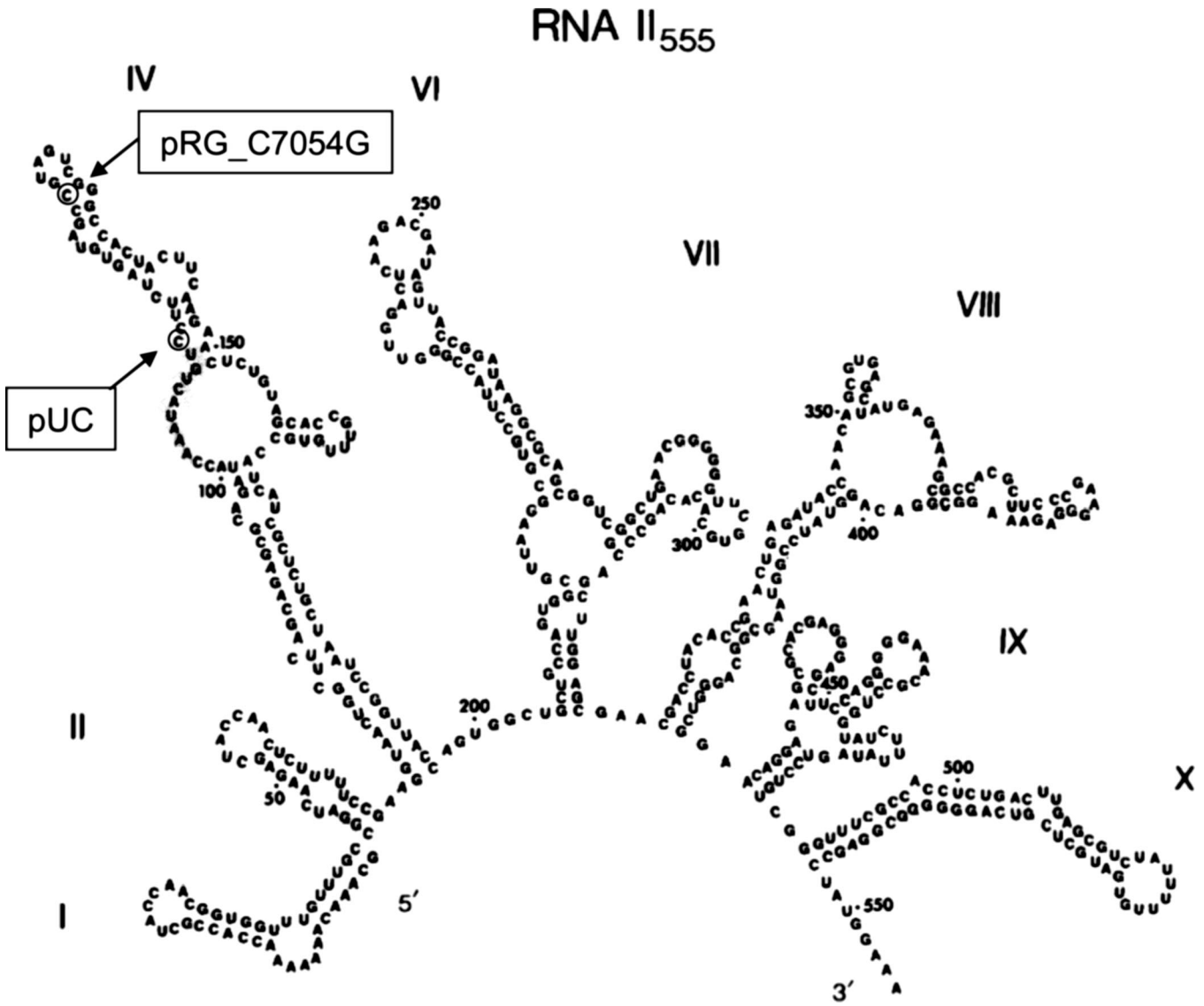

Fig. S15. Position of the mutation C7054G in the secondary structure of RNA II_{555} of ColE1-harboring plasmid pRG. The structural model shows that C7054G is positioned near the mutation that confers high levels of plasmid replication to pUC derived plasmids and close to the region which is complementary to the 5′ tail region of RNA I. [Reproduced with permission from ref. 1 (Copyright 1986, Elsevier).]

1. Tomizawa J (1986) Control of ColE1 plasmid replication: Binding of RNA I to RNA II and inhibition of primer formation. *Cell* 47:89–97.

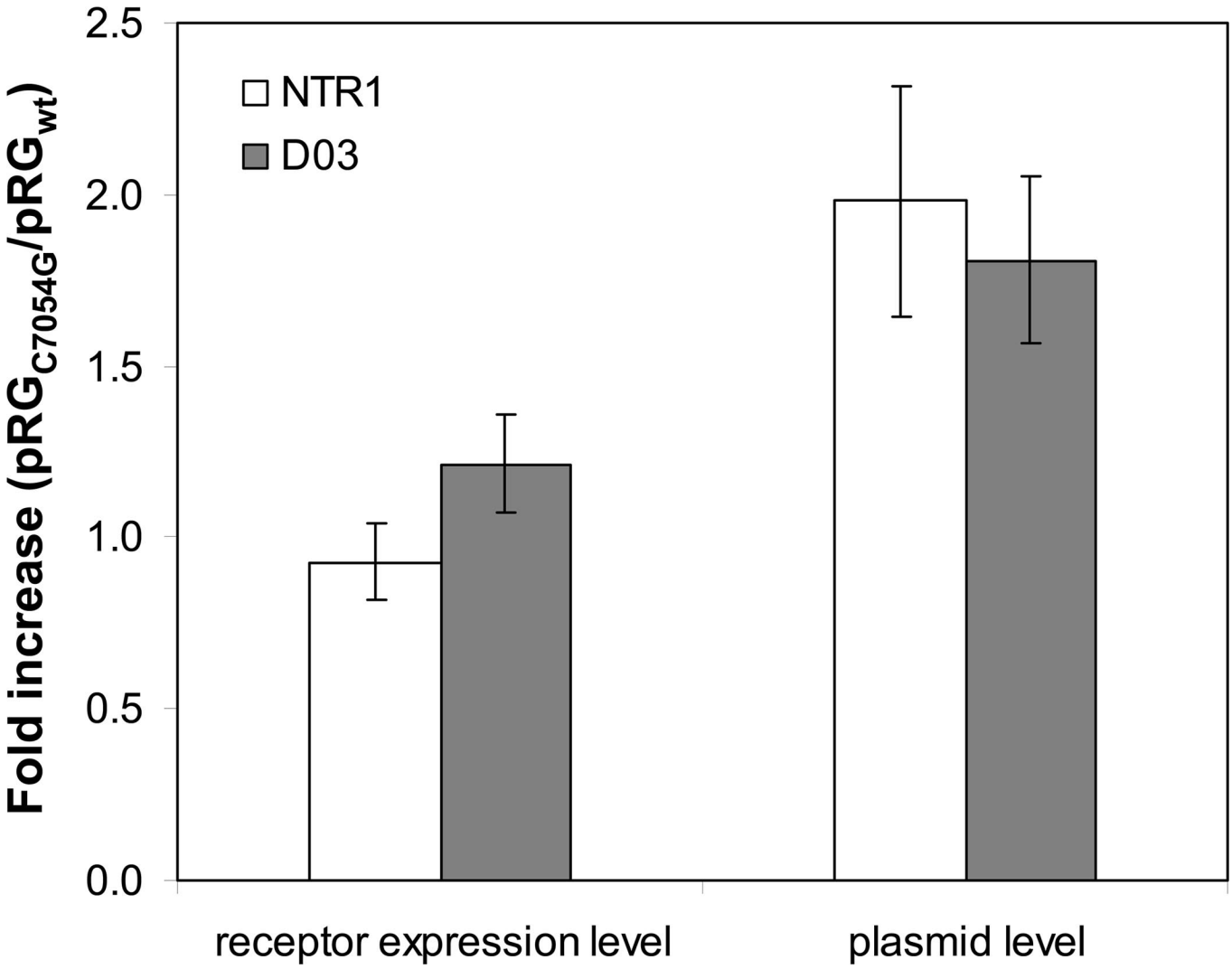

Fig. S16. Effect of the mutation C7054G in the origin of replication of the plasmid pRG on receptor expression and plasmid production levels in *E. coli*. C7054G leads to a twofold increase in plasmid content independent of the receptor gene cloned into the vector. However, when employing mutated plasmid pRG$_{C7054G}$, receptor expression increases for D03 but not for NTR1. All ratios were calculated based on data that had been normalized by OD_{600}.

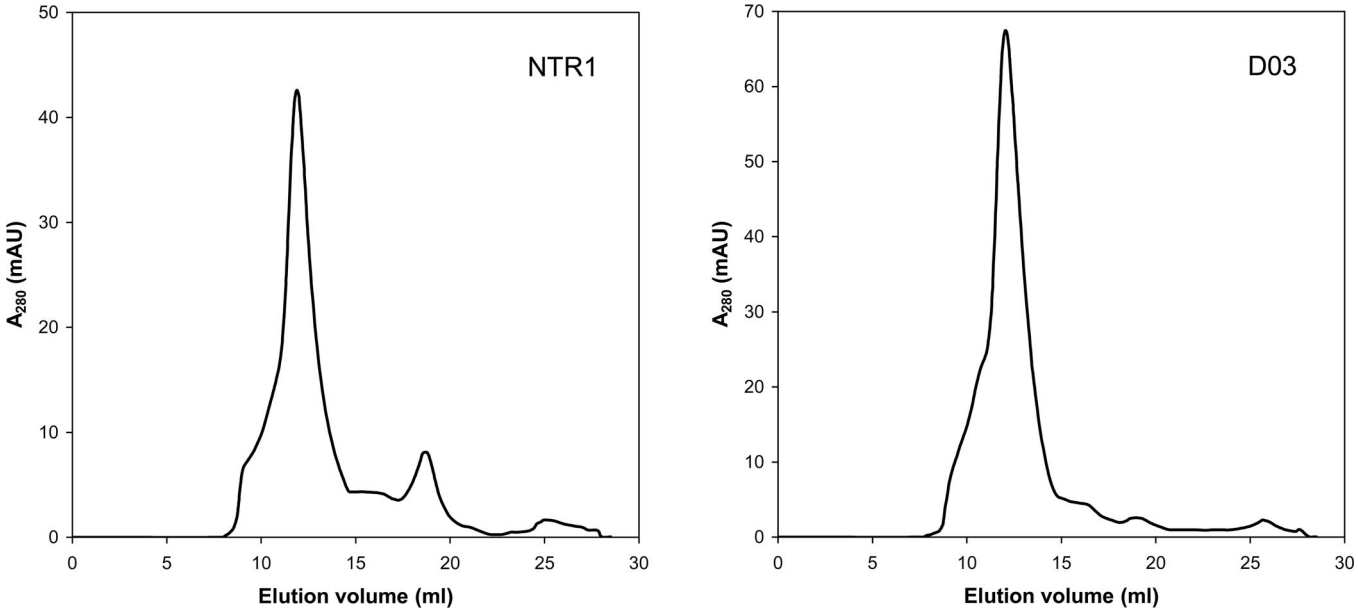

Fig. S17. Gel filtration profiles of NTR1 (*Left*; loaded 200 μg of functional receptor at 6.7 μM) and D03 (*Right*; loaded 310 μg of functional receptor at 10.4 μM). The main protein peak elutes at V_e = 11.9 ml and consists of functional receptor (see Fig. S18).

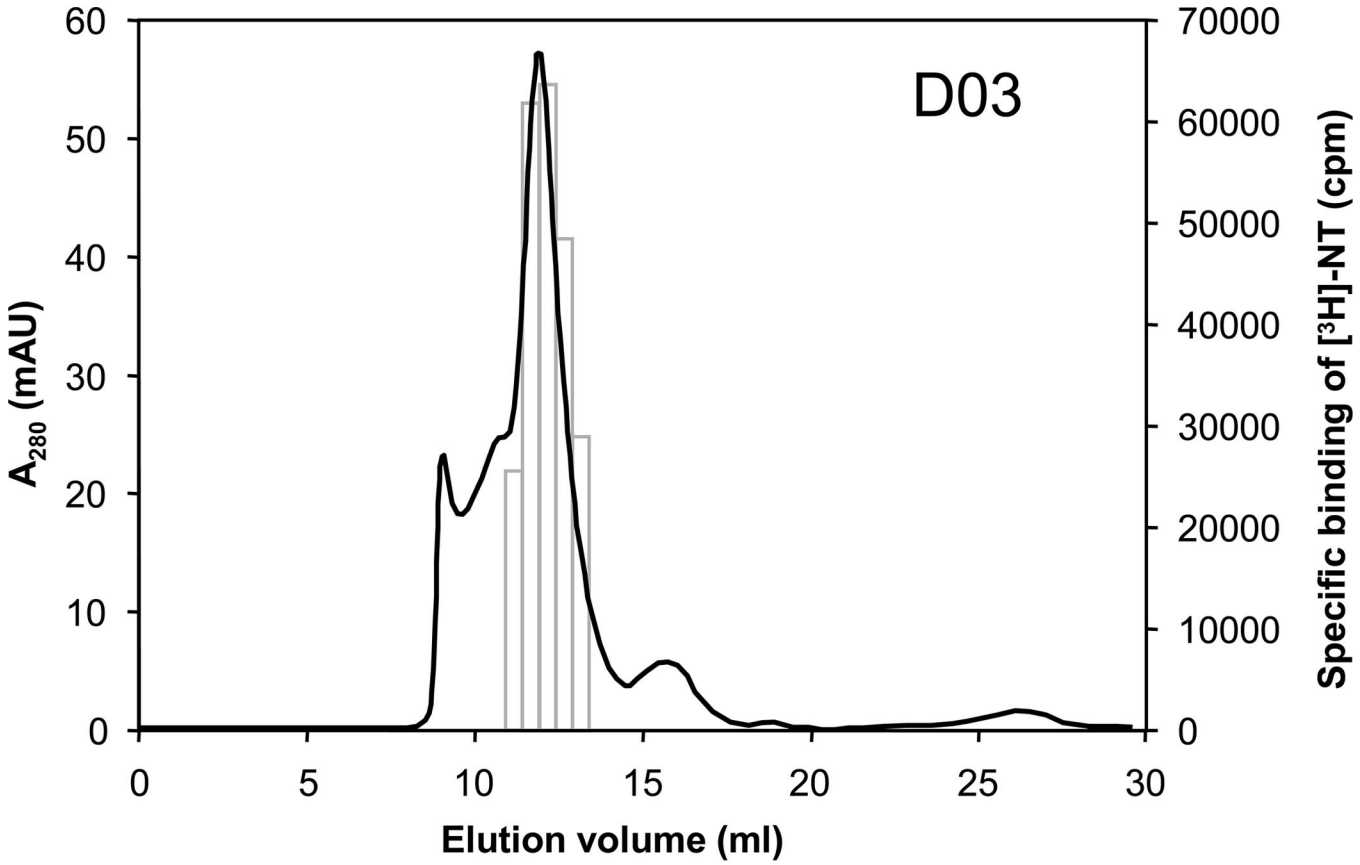

Fig. S18. Overlay of a D03 gel filtration profile (solid black line) and the corresponding functional receptor content of collected sample fractions as assessed by [^{3}H]-NT binding assays (open gray columns). The dominant peak (V_e = 11.9 ml) is the one that contains functional receptor.

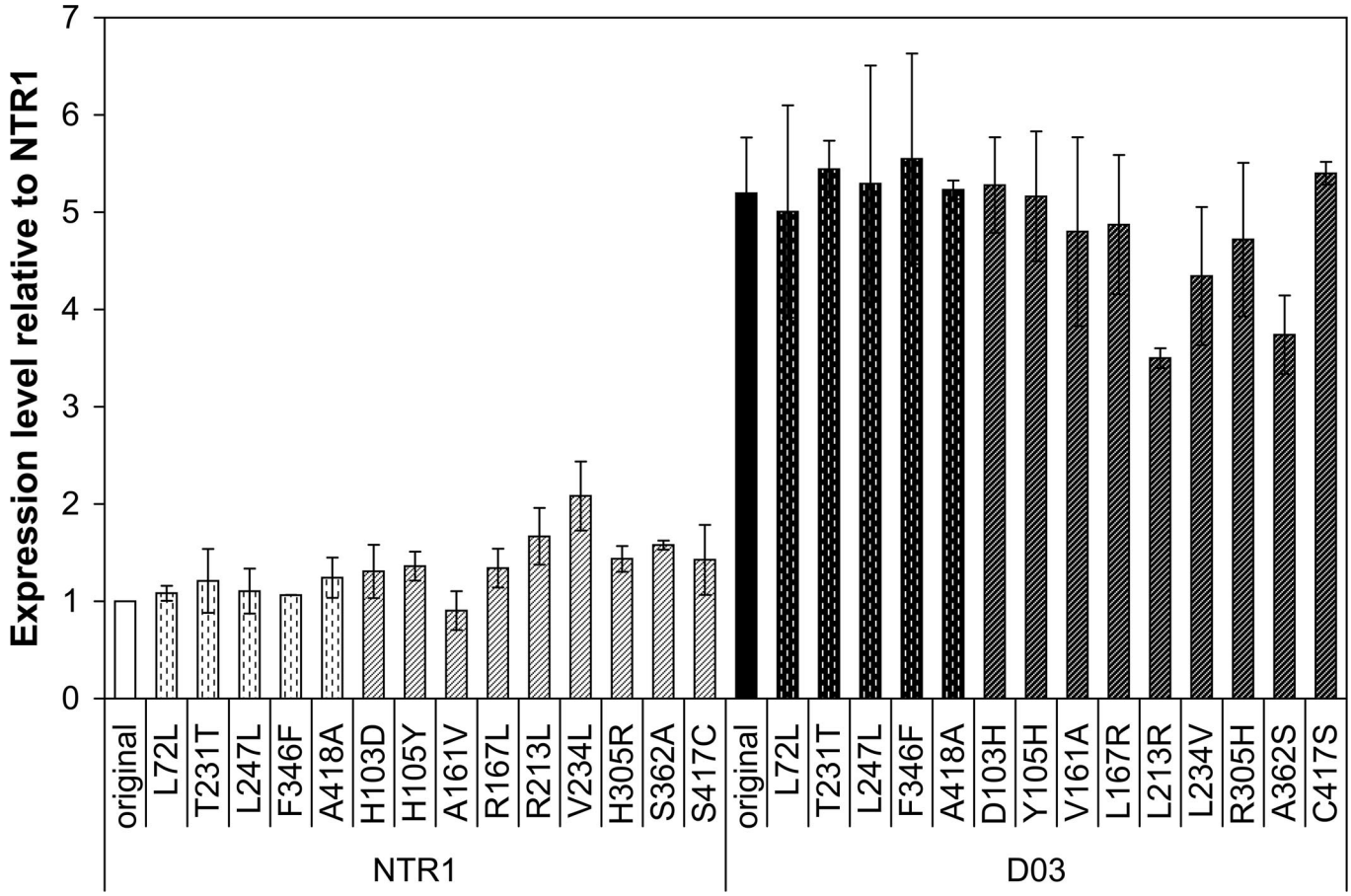

Fig. S19. Analysis of individual mutations in D03, which contains 14 nucleotide substitutions compared to NTR1. The first 15 columns in the graph represent NTR1 (solid white), 5 silent substitutions (vertical hash pattern), and 9 single-site mutants of WT that each introduces the evolved amino acid at that position in D03 (diagonal pattern). Likewise, the last 15 columns in the graph represent D03 (black bar), 5 silent substitutions (vertical hash pattern), and 9 single-site mutants of this GPCR that each reintroduces the corresponding WT amino acid (diagonal pattern). All constructs were expressed in the original expression vector lacking the backbone mutation (C7054G). Results represent three independent expression series.